Quiescent period respiratory gating for PET/CT

Chi Liu,[a] Adam Alessio, and Larry Pierce
Department of Radiology, University of Washington, Seattle, Washington 98195

Kris Thielemans
Hammersmith Imanet, GE Healthcare, London W12 ONN, United Kingdom

Scott Wollenweber and Alexander Ganin
GE Healthcare, Waukesha, Wisconsin 53188

Paul Kinahan
Department of Radiology, University of Washington, Seattle, Washington 98195

(Received 6 April 2010; revised 21 July 2010; accepted for publication 22 July 2010; published 30 August 2010)

Purpose: To minimize respiratory motion artifacts, this work proposes quiescent period gating (QPG) methods that extract PET data from the end-expiration quiescent period and form a single PET frame with reduced motion and improved signal-to-noise properties.
Methods: Two QPG methods are proposed and evaluated. Histogram-based quiescent period gating (H-QPG) extracts a fraction of PET data determined by a window of the respiratory displacement signal histogram. Cycle-based quiescent period gating (C-QPG) extracts data with a respiratory displacement signal below a specified threshold of the maximum amplitude of each individual respiratory cycle. Performances of both QPG methods were compared to ungated and five-bin phase-gated images across 21 FDG-PET/CT patient data sets containing 31 thorax and abdomen lesions as well as with computer simulations driven by 1295 different patient respiratory traces. Image quality was evaluated in terms of the lesion SUV_{max} and the fraction of counts included in each gate as a surrogate for image noise.
Results: For all the gating methods, image noise artifactually increases SUV_{max} when the fraction of counts included in each gate is less than 50%. While simulation data show that H-QPG is superior to C-QPG, the H-QPG and C-QPG methods lead to similar quantification-noise tradeoffs in patient data. Compared to ungated images, both QPG methods yield significantly higher lesion SUV_{max}. Compared to five-bin phase gating, the QPG methods yield significantly larger fraction of counts with similar SUV_{max} improvement. Both QPG methods result in increased lesion SUV_{max} for patients whose lesions have longer quiescent periods.
Conclusions: Compared to ungated and phase-gated images, the QPG methods lead to images with less motion blurring and an improved compromise between SUV_{max} and fraction of counts. The QPG methods for respiratory motion compensation could effectively improve tumor quantification with minimal noise increase. © *2010 American Association of Physicists in Medicine*.
[DOI: 10.1118/1.3480508]

Key words: respiratory motion correction, PET/CT, quiescent period

I. INTRODUCTION

Positron emission tomography/computed tomography (PET/CT) imaging of the lung and abdomen region is often affected by patient respiratory motion, which can lead to a tracer concentration underestimation of 30% or more, overestimation of tumor volume by a factor of 2 or more, and mismatched PET and CT images that subsequently cause errors in attenuation correction, registration and tumor localization.[1–5] Various motion compensation methods have been proposed and some of them, such as phase gating, have been implemented on clinical systems.

Respiratory-gated PET/CT divides PET data into different gates based on either temporal phase or respiratory displacement information with the potential for phase-matched CT-based attenuation correction.[6–16] Each gated frame contains less motion but higher image noise. The challenge with this approach is the increased noise per respiratory phase and the need for the physician to review all of the gated images. To achieve similar image noise as that in the ungated image, one can increase the acquisition time, which is not desirable in current clinical practice.[4] Depending on patient breathing patterns, the quality of images within different gates may not be comparable due to different degrees of intragate motion. For patients with irregular breathing patterns with amplitude variability, the gating methods, particularly those based on phase information, can give unsatisfactory results.[14]

Proposed motion compensation methods using all the detected coincident events typically start with respiratory-gated PET and/or CT data and incorporate estimated image-based motion information either into the image reconstruction[17–22] or postprocessing.[23–25] The image-based motion information used in these methods can be derived either from respiratory-

gated PET or CT images. Motion estimation from gated PET is subject to the high levels of image noise, leading to potential error in the estimated motion that can propagate into the motion corrected images. On the other hand, gated CT images have much lower noise, but the patient motion during CT imaging can be very different from the motion during PET imaging because of the respiratory variations between PET and CT acquisitions. Both of these approaches may require nonrigid volumetric image registration, which is sensitive to numerous free parameters and is computation-intensive.

Alternatives to gating are breath-hold PET/CT methods, which require patients to hold their breath during the PET and/or CT acquisition.[4,26–28] The breath-hold PET/CT images have less respiratory motion-blurring effects and more accurately aligned PET-CT images. However, this method is difficult to universally apply, as 40%–60% patients with lung cancer are unable to tolerate breath holding.[29]

Therefore, a motion correction method that allows free breathing, reduces motion blurring with minimal noise increase, but does not involve image-based motion estimation is desirable. Our previous analysis of 1295 patient respiratory traces showed that patients tend to spend more breathing time dwelling at the end-expiration quiescent period and breathe to the same end-expiration location.[5] These results indicate that imaging at end-expiration could include less motion while still retaining a large fraction of detected events. Based on these findings, we propose quiescent period gating (QPG) techniques that extract PET data from only the quiescent portions of patient breathing cycles to form a single PET image volume for physician review that has the optimal signal and noise tradeoff.

II. QUIESCENT PERIOD GATING METHODS

We developed and evaluated two quiescent period gating methods to extract PET data to form PET/CT images during the quiescent period of the patient's respiratory cycle. Both methods rely on external tracking of the respiratory motion. In this work, we used the Real-Time Position Management (RPM) gating system (Varian, Palo Alto, CA), which records the anterior-posterior (AP) chest displacement by optically tracking a reflective block marker.[30]

II.A. Histogram-based QPG method

The histogram-based method first histograms the respiratory trace displacement data, which records the anterior-posterior chest displacement and has arbitrary units determined by the RPM system. We then shift the displacement data so the displacement location that corresponds to the mode of trace histogram is set to zero. This provides the reference point. Next, the PET list mode data with trace displacement within a histogram window centered on the reference point are extracted to form the quiescent period gated data set. This histogram-based QPG (H-QPG) data set is reconstructed into the H-QPG image. The window is determined in such a way that the number of coincident events included in the window is a predefined fraction of the total number of detected events with the minimum displacement range within the window. For example, in Fig. 1(a), to include 40% of the event counts, the window was set around the histogram mode and the lower/upper boundaries were chosen to minimize the displacement differences within the window. This method allows the user to adjust the fraction of counts as a threshold to optimize the tradeoff between the intraframe motion and image noise.

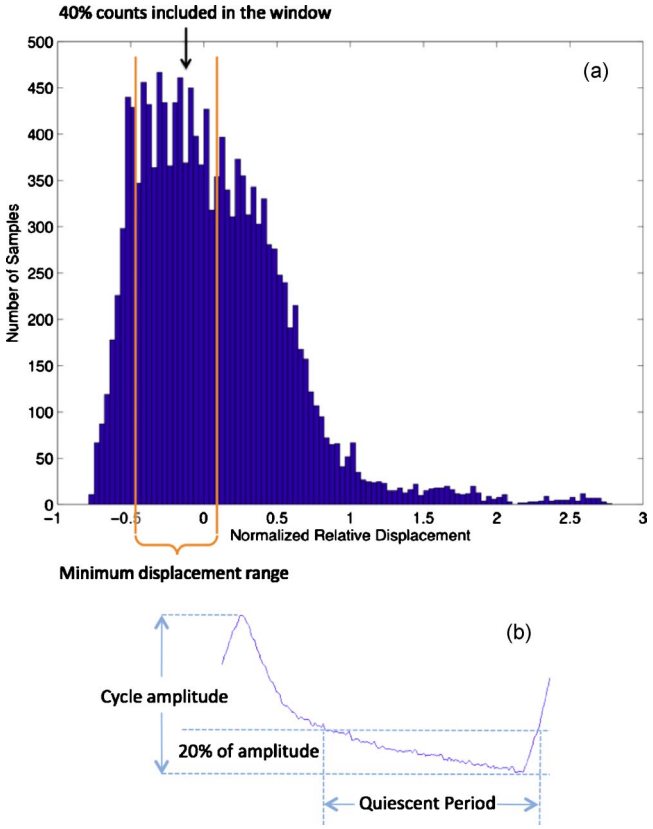

FIG. 1. (a) Illustration of histogram-based quiescent period gating. The histogram window contains 40% counts in this case. (b) Illustration of cycle-based quiescent period gating.

II.B. Cycle-base QPG method

As shown in Fig. 1(b), the cycle-based method extracts the PET list mode data below a certain percent threshold (e.g., 20%) of the amplitude in each cycle. This method relies on cycle-dependent amplitude calculation. The percent amplitude threshold for this method is parameterized, allowing different motion blur-noise tradeoffs.

III. METHODS AND MATERIALS

We compared the performance of the two quiescent period gating methods to the ungated and phase-gated (five-bin) PET images using a computer simulation study and pilot patient studies. For the cycle-based QPG (C-QPG) method, we evaluated five amplitude thresholds of 10%, 20%, 30%, 40%, and 50%. For the H-QPG method, the thresholds of fractions of counts for each QPG frame was chosen as 30%, 40%, 50%, 60%, and 70%.

III.A. Computer simulation

We collected 1295 patient respiratory traces using the RPM system during routine PET/CT studies at University of Washington Medical Center. We previously used these traces to drive a computer simulation package using the NURBS-based cardiac torso (NCAT) phantom to evaluate the impact of respiratory motion on static PET/CT quantification.[5] In the previous study, we have validated the simulation by comparing to a measured phantom experiment, where the respiratory motion of the phantom was driven with the same patient traces used in the simulation.[5] In this study, we used the same NCAT phantom whose diaphragm motion was driven by the RPM traces with 11 mm amplitude to generate motion-blurred data. Four lesions with 1 cm diameter and 8:1 contrast were inserted into upper lung, middle lung, lower lung, and liver regions.

By using the same data simulation methods, we generated the noise-free sinograms corresponding to the two quiescent period gating methods with different thresholds, five-bin phase gating, ungated acquisition, and motionless data for ground truth. All the simulated noise-free sinograms were reconstructed with OS-EM with four iterations and 20 subsets. Attenuation maps at end-expiration phases were used for attenuation correction. A Gaussian postfilter in transverse direction with 8 mm FWHM was applied. The SUV_{max} was measured as the maximum voxel value of each lesion and used for quantitative evaluation.

For each simulation and patient data below, we have computed the fraction of counts included in each gated image with respect to the ungated images, based on the corresponding durations of RPM trace signal. The fraction of counts is a surrogate of image noise, as larger fraction of counts leads to lower image noise.

For each reconstructed image, the change of lesion SUV_{max} with respect to that of the ungated images were analyzed as

$$\Delta SUV = \frac{SUV_{gated} - SUV_{ungated}}{SUV_{ungated}}, \quad (1)$$

where SUV_{gated} denotes the lesion SUV_{max} measured from one of the gated images of phase gating or QPG, as well as the motionless image in the simulation study. The $SUV_{ungated}$ denotes to the lesion SUV_{max} measured from ungated images. We assume that increased ΔSUV_{max} correlates with less respiratory motion and improved tracer quantification accuracy.

III.B. Patient studies

We evaluated the quiescent period gating methods with patient data acquired through an IRB-approved retrospective study. Patients were scheduled for routine FDG PET/CT study using GE DSTE PET/CT scanner (GE Healthcare, Waukesha, WI) operated in 2D mode at University of Washington Medical Center. The average injected dose was 10 mCi. In this study, we included patient data sets that had visible lesions in the lung and abdomen regions. All the lesions were confirmed by physicians to be potential tumors with focal FDG uptake. Patient data sets, whose RPM traces have operator errors, such as incorrect placement of optical tracking block, were excluded from the study. 21 patient data sets with a total number of 31 lesions were included in the study. Patient characteristics are summarized in Table I.

TABLE I. Characteristics of patients in this study. The study included 15 male and six female patients.

Characteristic	Mean ± SD	Range
Age (yr)	58.7 ± 8.5	45–75
Weight (kg)	78.9 ± 17.8	53–120
Height (cm)	174.4 ± 9.7	162–193
BMI	26.0 ± 5.1	15.8–35.8

For each patient, list mode data corresponding to a 7 min PET bed position containing lesions were binned to form sinograms for the different gating methods. All sinograms were reconstructed into $128 \times 128 \times 47$ image volumes with voxel size of $5.47 \times 5.47 \times 3.27$ mm^3 using the OS-EM algorithm using two iterations and 28 subsets. Corrections for attenuation, scatter, randoms, dead time, and detector efficiency normalization were included in the reconstruction. All the reconstructed images were smoothed with an 8 mm Gaussian postfilter. For each gating method with different parameter sets, the mean and standard deviation of ΔSUV_{max} and fraction of counts across all the 31 lesions were calculated and compared.

For QPG and phase-gating methods in this study, the gated images contained less counts than the ungated images and consequently had higher image noise. Image noise, due solely to poorer statistics, may lead to overestimation of ΔSUV_{max} in Eq. (1). To evaluate the impact of noise on lesion SUV_{max} change (ΔSUV_{max}) without any consideration for motion, we binned the PET list mode data by picking events separated by repeated short time intervals so that the binned sinograms had a smaller fraction of counts but retained the motion-blurring effect. We binned the data to have fractions of counts of 14%, 20%, 25%, 33%, 50%, 67%, 78%, 80%, and 87% and reconstructed them by using the same method for gated images. The lesion SUV_{max} change due solely to increased image noise was analyzed.

To study the impact of patient breathing pattern on SUV_{max} changes, we analyzed the shape of the displacement histogram of RPM trace of each patient. We classified traces into two groups: Those with a distinct displacement histogram peak at end-expiration and those without such a peak. As we have previously shown,[5] patients with a distinct histogram peak have a significant quiescent dwelling time and hence are expected to benefit more from quiescent period gating. The SUV_{max} changes of the two groups were then compared.

The statistical t-test was used to determine statistical significance of any difference in the patient study. The difference was considered statistically significant if the p-values were less than 0.05.

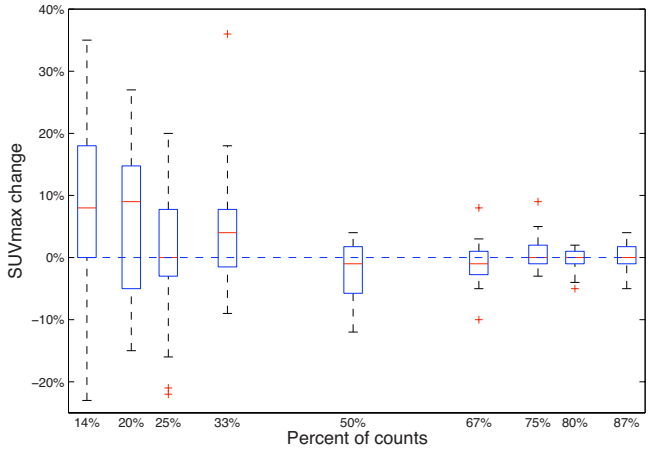

FIG. 2. SUV_{max} change as a function of fraction of counts for motion-blurred ungated patient data. The box stretches from the lower 25% quartile to the upper 75% quartile with a line across the box representing median. Whiskers extend from each end of the box to the most extreme values in the data within 1.5 times the interquartile range, which is defined as the difference between the upper quartile and the lower quartile, from each end of the box. Outliers with values beyond the ends of the whiskers are displayed with a + sign.

IV. RESULTS

IV.A. Impact of image noise on SUV

Tumor SUV_{max} changes as a function of fraction of counts in ungated patient data are presented in Fig. 2. With fractions of counts 50% or larger, the medians of ΔSUV_{max} were close to 0% and their variances were small. Both the median and variance of ΔSUV_{max} was larger for fractions of counts smaller than 50%. Particularly for 20% fraction of counts, where the five-bin phase gating operates, the noise alone caused a median of 9% overestimation on SUV_{max}.

IV.B. Impact of QPG methods on SUV

Sample patient coronal images in Fig. 3 revealed that both H-QPG and C-QPG reduced respiratory blurring with respect to ungated image. Compared to the gate 3 of phase gating, both QPG methods gave images with a similar reduction in the blurring effect but with less image noise.

Figure 4 summarizes the results from computer simulation and patient studies with different thresholds. In the simulation results shown in Fig. 4(a), for the middle lung lesion as an example, the averaged five-bin phase gating, based on 1295 patient traces, had an inferior trade-off between ΔSUV_{max} and fraction of counts as compared to the QPG methods. The histogram-based QPG, on average, gave consistently larger ΔSUV_{max} compared to the cycle-based QPG. The motionless image, which corresponds to a hypothetically perfect motion correction method, gave the highest ΔSUV_{max} of $37.8\% \pm 17.4\%$. As shown in Fig. 4(b) with patient data, the histogram-based and cycle-based QPG method curves nearly overlap and both have a superior trade-off between ΔSUV_{max} and fraction of counts compared to five-bin phase gating. Compared to phase gating, all the H-QPG and C-QPG methods with different thresholds lead to significantly larger fraction of counts with p-values smaller than 0.01. In the patient study, the differences in ΔSUV_{max} between QPG and phase gating were not proven to be significant for any case with p-values ranging between 0.21 and 0.95 for different thresholds. Compared to ungated images, all the QPG methods with different thresholds lead to significantly larger SUV_{max} with p-values smaller than 0.001.

TABLE II. Means, SDs, and statistical tests of ΔSUV max for the QPG methods with sample thresholds stratified by breathing types. (QP: With a distinct quiescent peak at end-expiration; non-QP: Without distinct quiescent peaks.) p-values <0.05 are considered statistically significant.

Breathing types	H-QPG w/50% counts	C-QPG w/20% threshold
QP (N=20)	$11.5\% \pm 14.2\%$	$11.0\% \pm 13.1\%$
Non-QP (N=11)	$4.7\% \pm 4.7\%$	$6.5\% \pm 6.3\%$
p-value	0.13	0.30

As shown in Table II, patients whose RPM trace histograms had a distinct quiescent peak at end-expiration had larger SUV_{max} changes compared to those of patients whose RPM traces do not have a quiescent peak, but the differences were not statistically significant.

V. DISCUSSION

We proposed histogram-based and cycle-based quiescent period gating methods and evaluated their performance using 21 patient data sets with 31 lesions and a computer simulation driven by a large number of patient respiratory traces. The rationale of quiescent period gating was to take the patient breathing pattern into account and form a single frame with minimal respiratory motion and low image noise from the portion of the respiratory cycle with the least motion.

In Figs. 4(a) and 4(b), the upper-right corner of the plot with larger SUV_{max} change and larger fraction of counts corresponds to a superior image quality with less motion and lower noise. Compared to the phase gating, the curves of the quiescent period gating methods are more toward the upper-right corner, indicating superior image quality. In Fig. 4(a), the difference between QPG and motionless indicated that the QPG methods effectively reduced motion blurring without causing SUV overestimation. The differences in ΔSUV_{max} between the motionless case and QPG methods are due to the fact that each quiescent period still contains residual intragate motion.

Compared to the ungated images using all the detected counts, the quiescent period gating methods and five-bin phase gating contain only a fraction of the total detected events. Therefore, each gated image is noisier than the ungated image and this noise will have an impact on the SUV_{max} measurement. As shown in Fig. 2, the median and variance of ΔSUV_{max} became much larger for fractions of counts smaller than 50%. Particularly for the 20% fraction of counts, as with the five-bin phase gating, the noise alone can lead to a median 9% ΔSUV_{max} and at worst a 27% ΔSUV_{max}. This result was derived from the particular patient

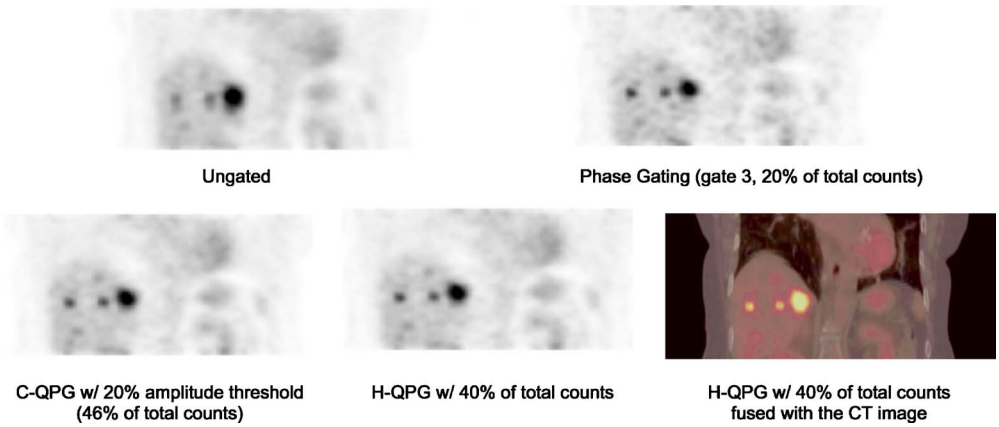

FIG. 3. Sample coronal patient images from different methods. Both phase-gating and QPG methods lead to less-blurred images. The images using QPG methods have lower image noise than phase gating.

data set used in this study. The general trend that shows higher image noise causes larger SUV_{max} overestimation can be generalized. However, the exact quantitative numbers in other studies may be different and highly depend on the image noise, which is determined by factors such as total acquisition time, 2D or 3D acquisition mode, and reconstruction and filter parameters.

Thus, in Fig. 4(b), the increased ΔSUV_{max} for phase gating is due to a combination of increased noise and motion correction. But for both QPG methods, the increased ΔSUV_{max} primarily comes from motion correction with minimal contribution from noise increase. According to the statistical test, both QPG methods use significantly larger fractions of counts to achieve nonsignificant ΔSUV_{max} difference as compared to phase gating. These statistical test results indicate that QPG methods can give equivalent motion correction as compared to phase gating, but images have much lower noise and thus higher image quality.

Recently, temporal phase gating has become available in some clinical PET/CT scanners. We used this capability to develop a pragmatic implement of quiescent period gating. For a typical patient breathing curve with five-bin phase gating, gates 3 and 4 roughly correspond to quiescent period and have less motion than gates 1 and 5. Thus we combined the sinograms of gates 3 and 4 and reconstructed the combined sinogram to form a single frame as a potential surrogate of quiescent period gating, containing 40% of the events. As shown in Fig. 4(b), the trade-off performance of combined gates 3 and 4 is very close to that of quiescent period gating. Therefore, combining gates 3 and 4 may be a pragmatic implementation of quiescent period gating for current clinical scanners. To refine this approach, it may be desirable to bin the data into a larger number of frames, such as eight or ten, and combine the gates corresponding to the quiescent period with a greater flexibility.

In Table II, quiescent period gating leads to an improvement, but nonsignificant due to the relatively small sample size, for patients who spend more time breathing around end-expiration (quiescent period phase). This indicated that although intuitively QPG methods would benefit most for the patients with larger quiescent period fraction, the QPG methods could also make universal improvement for patients with other breathing patterns.

For patients with very regular breathing patterns without much end-expiration variation, both the histogram-based and cycle-based methods should lead to similar improvements. However, for the traces with significant variations on amplitude and end-expiration location, if the internal tumor motion correlates well with the external chest AP motion,[31–34] the histogram-based method is expected to yield images with less motion than the cycle-based method. In noise-free simulations [Fig. 4(a)], the curves of histogram-based QPG are consistently higher than those of cycle-base QPG. But this is not the case in measured patient data [Fig. 4(b)], where the curves of both QPG methods roughly overlap. This discrepancy may be due to the assumptions in the computer simulation. We used the patient RPM traces to drive the diaphragm motion of the phantom. Therefore the external-internal displacement correlation is perfect in our computer simulation and the histogram-based method outperforms the cycle-based methods for RPM traces with major respiratory signal variations on amplitude and end-expiration location. Studying patient data, however, we do not have exact knowledge of the internal-external displacement correlations. That is, the absolute internal tumor location may be different for the same RPM displacement. In this case we would not expect to see a significant advantage for the histogram-based methods. However, if we can find a way to directly estimate internal tumor motion traces in a reliable way, as is demonstrated as feasible in Refs. 35–40, we may use internal motion traces to guide respiratory gating, which would retain the advantage of the histogram-based method over cycle-based methods. Another consideration is that the histogram-based QPG requires the entire respiratory trace histogram and therefore must be applied as a retrospective gating method. In contrast, the cycle-based QPG can bin the data prospectively, allowing real time binning during data acquisition to potentially save postprocessing time.

In each patient data set, a helical CT image was acquired during free breathing with the current clinical protocol at

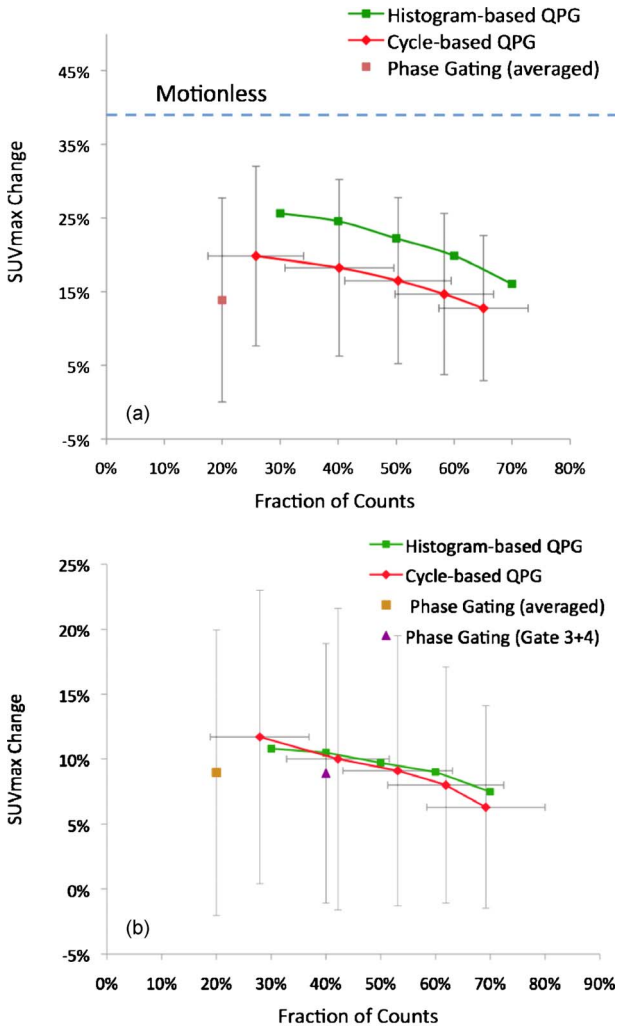

FIG. 4. ΔSUV_{max} as a function of fraction of counts for different gating methods in (a) simulation study and (b) patient study. In the simulation study, the ΔSUV_{max} for the motionless data is $37.8\% \pm 17.4\%$. For visual clarity, the variances are not shown for histogram-based QPG, which does not have variances regarding the fraction of counts. The magnitudes of variances of histogram-based and cycle-based QPGs regarding the ΔSUV_{max} are similar. In the patient study, statistical test showed that compared to phase gating, all the QPG methods with different thresholds do not have significant difference on ΔSUV_{max} with p-value range of 0.21–0.95, but all have significantly larger fraction of counts with p-values smaller than 0.001.

University of Washington. Therefore, the CT image corresponds to an arbitrary breathing location. With CT-based attenuation correction, this may lead to a larger improvement of SUV_{max} in a particular phase frame if PET/CT images match better, but smaller improvement in other frames with more severe PET/CT mismatch, both in phase gating and quiescent period gating. This may confound the results and is a limitation in this study. Phase-matched attenuation correction would offer the most accurate PET quantification. With cine CT acquired, a weighted-averaged CT image corresponding to quiescent period of the selected PET data could be generated. This quiescent period CT image has the potential to be nearly matched with the quiescent phase PET data for accurate attenuation correction. Such evaluation needs further study.

The QPG methods are intended for patients under free breathing. They extract data from quiescent periods generally during end tidal expiration with smaller lung volumes as compared to end-inspiration. The expanded lung volume of end-inspiration may improve the ability to detect small lung lesions and represents one of the rationales for alternative methods such as deep-inspiration breath-hold PET/CT.[26,27] Using similar arguments, the expanded abdominal space during end-expiration may improve the ability to detect abdominal lesions. To the best of our knowledge, it has not been shown which respiratory phase is optimal for lesion detection with PET imaging.

VI. CONCLUSIONS

Quiescent period gating methods have the potential to improve PET image quality in clinical studies by reducing the respiratory motion effect with minimum image noise increase. Compared to conventional phase gating, quiescent period gating methods lead to an improved compromise between motion degradation and image noise.

ACKNOWLEDGMENTS

This work is funded by NIH Grant No. R01-CA115870 and a research contract from GE Healthcare. The authors would like to thank Jenine Yager for coordinating the patient study. Thanks also go to Ravindra Manjeshwar from GE Global Research and Steve Kohlmyer from GE Healthcare for helpful discussions.

[a]Electronic mail: chi.liu@yale.edu

[1]Y. E. Erdi, S. A. Nehmeh, T. Pan, A. Pevsner, K. E. Rosenzweig, G. Mageras, E. D. Yorke, H. Schoder, W. Hsiao, O. D. Squire, P. Vernon, J. B. Ashman, H. Mostafavi, S. M. Larson, and J. L. Humm, "The CT motion quantitation of lung lesions and its impact on PET-measured SUVs," J. Nucl. Med. **45**, 1287–1292 (2004).
[2]B. Thorndyke, E. Schreibmann, A. Koong, and L. Xing, "Reducing respiratory motion artifacts in positron emission tomography through retrospective stacking," Med. Phys. **33**, 2632–2641 (2006).
[3]S. A. Nehmeh and Y. E. Erdi, "Respiratory motion in positron emission tomography/computed tomography: A review," Semin Nucl. Med. **38**, 167–176 (2008).
[4]T. Kawano, E. Ohtake, and T. Inoue, "Deep-inspiration breath-hold PET/CT of lung cancer: Maximum standardized uptake value analysis of 108 patients," J. Nucl. Med. **49**, 1223–1231 (2008).
[5]C. Liu, L. Pierce, A. M. Alessio, and P. E. Kinahan, "The impact of respiratory motion on tumor quantification and delineation in static PET/CT imaging," Phys. Med. Biol. **54**, 7345–7362 (2009).
[6]S. A. Nehmeh, Y. E. Erdi, T. Pan, A. Pevsner, K. E. Rosenzweig, E. Yorke, G. S. Mageras, H. Schoder, P. Vernon, O. Squire, H. Mostafavi, S. M. Larson, and J. L. Humm, "Four-dimensional (4D) PET/CT imaging of the thorax," Med. Phys. **31**, 3179–3186 (2004).
[7]S. A. Nehmeh, Y. E. Erdi, T. Pan, E. Yorke, G. S. Mageras, K. E. Rosenzweig, H. Schoder, H. Mostafavi, O. Squire, A. Pevsner, S. M. Larson, and J. L. Humm, "Quantitation of respiratory motion during 4D-PET/CT acquisition," Med. Phys. **31**, 1333–1338 (2004).
[8]T. Pan, T. Y. Lee, E. Rietzel, and G. T. Chen, "4D-CT imaging of a volume influenced by respiratory motion on multi-slice CT," Med. Phys. **31**, 333–340 (2004).
[9]E. Rietzel, T. Pan, and G. T. Chen, "Four-dimensional computed tomography: Image formation and clinical protocol," Med. Phys. **32**, 874–889 (2005).
[10]J. W. Wolthaus, M. van Herk, S. H. Muller, J. S. Belderbos, J. V. Lebesque, J. A. de Bois, M. M. Rossi, and E. M. Damen, "Fusion of respiration-correlated PET and CT scans: Correlated lung tumour motion

in anatomical and functional scans," Phys. Med. Biol. **50**, 1569–1583 (2005).
[11]W. Lu, P. J. Parikh, J. P. Hubenschmidt, J. D. Bradley, and D. A. Low, "A comparison between amplitude sorting and phase-angle sorting using external respiratory measurement for 4D CT," Med. Phys. **33**, 2964–2974 (2006).
[12]N. Wink, C. Panknin, and T. D. Solberg, "Phase versus amplitude sorting of 4D-CT data," J. Appl. Clin. Med. Phys. **7**, 77–85 (2006).
[13]T. Pan, X. Sun, and D. Luo, "Improvement of the cine-CT based 4D-CT imaging," Med. Phys. **34**, 4499–4503 (2007).
[14]A. F. Abdelnour, S. A. Nehmeh, T. Pan, J. L. Humm, P. Vernon, H. Schoder, K. E. Rosenzweig, G. S. Mageras, E. Yorke, S. M. Larson, and Y. E. Erdi, "Phase and amplitude binning for 4D-CT imaging," Phys. Med. Biol. **52**, 3515–3529 (2007).
[15]M. Dawood, F. Buther, N. Lang, O. Schober, and K. P. Schafers, "Respiratory gating in positron emission tomography: A quantitative comparison of different gating schemes," Med. Phys. **34**, 3067–3076 (2007).
[16]M. Guckenberger, M. Weininger, J. Wilbert, A. Richter, K. Baier, T. Krieger, B. Polat, and M. Flentje, "Influence of retrospective sorting on image quality in respiratory correlated computed tomography," Radiother. Oncol. **85**, 223–231 (2007).
[17]T. Li, B. Thorndyke, E. Schreibmann, Y. Yang, and L. Xing, "Model-based image reconstruction for four-dimensional PET," Med. Phys. **33**, 1288–1298 (2006).
[18]R. Manjeshwar, X. Tao, E. Asma, and K. Thielemans, "Motion compensated image reconstruction of respiratory gated PET/CT," in Proceedings of the Third IEEE International Symposium on Biomedical Imaging, 2006, pp. 674–677.
[19]F. Qiao, T. Pan, J. W. J. Clark, and O. R. Mawlawi, "A motion-incorporated reconstruction method for gated PET studies," Phys. Med. Biol. **51**, 3769–3783 (2006).
[20]F. Lamare, M. J. Ledesma Carbayo, T. Cresson, G. Kontaxakis, A. Santos, C. C. Le Rest, A. J. Reader, and D. Visvikis, "List-mode-based reconstruction for respiratory motion correction in PET using non-rigid body transformations," Phys. Med. Biol. **52**, 5187–5204 (2007).
[21]F. Qiao, T. Pan, J. W. Clark, and O. R. Mawlawi, "Region of interest motion compensation for PET image reconstruction," Phys. Med. Biol. **52**, 2675–2689 (2007).
[22]F. Qiao, T. Pan, J. W. J. Clark, and O. Mawlawi, "Joint model of motion and anatomy for PET image reconstruction," Med. Phys. **34**, 4626–4639 (2007).
[23]M. Dawood, N. Lang, X. Jiang, and K. P. Schafers, "Lung motion correction on respiratory gated 3-D PET/CT images," IEEE Trans. Med. Imaging **25**, 476–485 (2006).
[24]T. Yamazaki, H. Ue, H. Haneishi, A. Hirayama, T. Sato, and S. Nawano, "An attenuation correction method for respiratory-gated PET/CT image," in IEEE Nuclear Science Symposium Conference Record, 2006.
[25]P. E. Kinahan, S. Wollenweber, A. M. Alessio, S. Kohlmyer, L. MacDonald, T. K. Lewellen, and A. Ganin, "Impact of respiration variability on respiratory gated whole-body PET/CT imaging," J. Nucl. Med. **48**, 196 (2007).
[26]G. S. P. Meirelles, Y. E. Erdi, S. A. Nehmeh, O. D. Squire, S. M. Larson, J. L. Humm, and H. Schoder, "Deep-inspiration breath-hold PET/CT: Clinical findings with a new technique for detection and characterization of thoracic lesions," J. Nucl. Med. **48**, 712–719 (2007).
[27]S. A. Nehmeh, Y. E. Erdi, G. S. P. Meirelles, O. Squire, S. M. Larson, J. L. Humm, and H. Schoder, "Deep-inspiration breath-hold PET/CT of the thorax," J. Nucl. Med. **48**, 22–26 (2007).
[28]T. Torizuka, Y. Tanizaki, T. Kanno, M. Futatsubashi, E. Yoshikawa, H. Okada, and Y. Ouchi, "Single 20-second acquisition of deep-inspiration breath-hold PET/CT: Clinical feasibility for lung cancer," J. Nucl. Med. **50**, 1579–1584 (2009).
[29]S. Senan, D. De Ruysscher, P. Giraud, R. Mirimanoff, and V. Budach, "Literature-based recommendations for treatment planning and execution in high-dose radiotherapy for lung cancer," Radiother. Oncol. **71**, 139–146 (2004).
[30]S. S. Vedam, V. R. Kini, P. J. Keall, V. Ramakrishnan, H. Mostafavi, and R. Mohan, "Quantifying the predictability of diaphragm motion during respiration with a noninvasive external marker," Med. Phys. **30**, 505–513 (2003).
[31]A. S. Beddar, K. Kainz, T. M. Briere, Y. Tsunashima, T. Pan, K. Prado, R. Mohan, M. Gillin, and S. Krishnan, "Correlation between internal fiducial tumor motion and external marker motion for liver tumors imaged with 4D-CT," Int. J. Radiat. Oncol., Biol., Phys. **67**, 630–638 (2007).
[32]D. P. Gierga, J. Brewer, G. C. Sharp, M. Betke, C. G. Willett, and G. T. Chen, "The correlation between internal and external markers for abdominal tumors: Implications for respiratory gating," Int. J. Radiat. Oncol., Biol., Phys. **61**, 1551–1558 (2005).
[33]J. D. Hoisak, K. E. Sixel, R. Tirona, P. C. Cheung, and J. P. Pignol, "Correlation of lung tumor motion with external surrogate indicators of respiration," Int. J. Radiat. Oncol., Biol., Phys. **60**, 1298–1306 (2004).
[34]D. Ionascu, S. B. Jiang, S. Nishioka, H. Shirato, and R. I. Berbeco, "Internal-external correlation investigations of respiratory induced motion of lung tumors," Med. Phys. **34**, 3893–3903 (2007).
[35]R. A. Bundschuh, A. Martinez-Moeller, M. Essler, M. J. Martinez, S. G. Nekolla, S. I. Ziegler, and M. Schwaiger, "Postacquisition detection of tumor motion in the lung and upper abdomen using list-mode PET data: A feasibility study," J. Nucl. Med. **48**, 758–763 (2007).
[36]F. Buther, M. Dawood, L. Stegger, F. Wubbeling, M. Schafers, O. Schober, and K. P. Schafers, "List mode-driven cardiac and respiratory gating in PET," J. Nucl. Med. **50**, 674–681 (2009).
[37]A. L. Kesner, R. A. Bundschuh, N. C. Detorie, M. Dahlbom, S. I. Ziegler, J. Czernin, and D. H. Silverman, "Respiratory gated PET derived in a fully automated manner from raw PET data," IEEE Trans. Nucl. Sci. **56**, 677–686 (2009).
[38]G. J. Klein, B. W. Reutter, E. H. Botvinick, T. F. Budinger, and R. H. Juesman, "Fine-scale motion detection using intrinsic list mode PET information," in IEEE Nuclear Science Symposium Conference Record, 2001.
[39]P. J. Schleyer, M. J. O'Doherty, S. F. Barrington, and P. K. Marsden, "Retrospective data-driven respiratory gating for PET/CT," Phys. Med. Biol. **54**, 1935–1950 (2009).
[40]D. Visvikis, O. Barret, T. Fryer, A. Turzo, F. Lamare, C. Cheze Le Rest, and Y. Bizais, "A posteriori respiratory motion gating of dynamic PET images," in IEEE Nuclear Science Symposium Conference Record, 2003, Vol. 5, pp. 3276–3280.